Development 138, 45-54 (2011) doi:10.1242/dev.052985

The Rho kinase Rock2b establishes anteroposterior asymmetry of the ciliated Kupffer's vesicle in zebrafish

Guangliang Wang[1], Adam B. Cadwallader[2,*], Duck Soo Jang[1], Michael Tsang[3], H. Joseph Yost[2] and Jeffrey D. Amack[1,†]

SUMMARY

The vertebrate body plan features a consistent left-right (LR) asymmetry of internal organs. In several vertebrate embryos, motile cilia generate an asymmetric fluid flow that is necessary for normal LR development. However, the mechanisms involved in orienting LR asymmetric flow with previously established anteroposterior (AP) and dorsoventral (DV) axes remain poorly understood. In zebrafish, asymmetric flow is generated in Kupffer's vesicle (KV). The cellular architecture of KV is asymmetric along the AP axis, with more ciliated cells densely packed into the anterior region. Here, we identify a Rho kinase gene, *rock2b*, which is required for normal AP patterning of KV and subsequent LR development in the embryo. Antisense depletion of *rock2b* in the whole embryo or specifically in the KV cell lineage perturbed asymmetric gene expression in lateral plate mesoderm and disrupted organ LR asymmetries. Analyses of KV architecture demonstrated that *rock2b* knockdown altered the AP placement of ciliated cells without affecting cilia number or length. In control embryos, leftward flow across the anterior pole of KV was stronger than rightward flow at the posterior end, correlating with the normal AP asymmetric distribution of ciliated cells. By contrast, *rock2b* knockdown embryos with AP patterning defects in KV exhibited randomized flow direction and equal flow velocities in the anterior and posterior regions. Live imaging of *Tg*(*dusp6:memGFP*)^{pt19} transgenic embryos that express GFP in KV cells revealed that *rock2b* regulates KV cell morphology. Our results suggest a link between AP patterning of the ciliated Kupffer's vesicle and LR patterning of the zebrafish embryo.

KEY WORDS: Left-right patterning, Cilia, Rho kinase, Kupffer's vesicle, Zebrafish development

INTRODUCTION

Disruption of organ left-right (LR) asymmetry, or laterality, during embryo development can result in birth defects, which often include complex congenital heart defects (Ramsdell, 2005). Asymmetric expression of *nodal*, *lefty* and *pitx2* gene family members in left lateral plate mesoderm (LPM) is crucial for normal organ laterality in vertebrates (reviewed in Hamada et al., 2002; Raya and Belmonte, 2006; Yost, 1999). The initiation of this asymmetric Nodal-Lefty-Pitx2 cascade must be properly aligned with pre-existing anteroposterior (AP) and dorsoventral (DV) axes. A group of motile monocilia (we refer to as 'LR cilia') found on epithelia at the ventral node in mouse (Nonaka et al., 1998), notochordal plate in rabbit (Okada et al., 2005), gastrocoel roof plate in frog (Schweickert et al., 2007) and Kupffer's vesicle (KV) in medaka (Okada et al., 2005) and zebrafish (Essner et al., 2005; Kramer-Zucker et al., 2005) generate a directional fluid flow that is required for biasing Nodal-Lefty-Pitx2 expression to the left LPM. The involvement of cilia-driven flow in LR patterning suggests the relative position of LR ciliated cells in the embryo is under tight genetic control and plays an important role in orienting the LR axis with the AP and DV axes. However, signaling pathways and molecular mechanisms involved in establishing the architecture of the LR ciliated epithelium are poorly understood.

In the mouse embryo, LR cilia use a rotational stroke to create a right-to-left fluid flow (Nonaka et al., 1998). This leftward flow is probably a result of posterior tilting of the cilia (Nonaka et al., 2005; Okada et al., 2005). Mutant mice indicate cilium tilt is controlled by positioning of the basal body in the posterior region of the cell, which is regulated by planar cell polarity (PCP) signaling (Antic et al., 2010; Hashimoto et al., 2010; Okada et al., 2005; Song et al., 2010). Posterior projection of LR cilia has also been observed in frog (Schweickert et al., 2007), medaka (Okada et al., 2005) and zebrafish (Kramer-Zucker et al., 2005; Okabe et al., 2008). A recent report suggests that relative positioning of cells in the ciliated epithelium contributes to the posterior projection of LR cilia in zebrafish (Okabe et al., 2008), and potentially other vertebrates.

In zebrafish, LR cilia produce asymmetric flow in KV (Essner et al., 2005; Kramer-Zucker et al., 2005). Dorsal forerunner cells (DFCs) are precursors of KV cells (Cooper and D'Amico, 1996; Melby et al., 1996) that migrate ahead of the dorsal blastoderm margin during gastrulation and then differentiate into ciliated epithelial KV cells at the end of epiboly (Amack et al., 2007; Oteiza et al., 2008). Importantly, LR ciliated cells are not equally distributed in KV. Immunostaining and histological studies (Kreiling et al., 2007; Okabe et al., 2008) have revealed that there are more cilia on the dorsal 'roof' than the posterior 'floor' and that more ciliated cells are positioned in the anterior region than in the posterior region of KV. The asymmetric AP distribution of LR cilia results in a dense clustering of cilia in the anterior pole of KV which project posteriorly, and may be the driving force behind directional flow; it has been observed that flow is stronger from

[1]Department of Cell and Developmental Biology, State University of New York, Upstate Medical University, Syracuse, NY 13210, USA. [2]Department of Neurobiology and Anatomy, University of Utah School of Medicine, Salt Lake City, UT 84112, USA. [3]Department of Developmental Biology, University of Pittsburgh School of Medicine, Pittsburgh, PA 15213, USA.

*Present address: Department of Molecular, Cellular and Developmental Biology, University of Colorado, Boulder, CO 80309, USA
†Author for correspondence (amackj@upstate.edu)

Accepted 28 October 2010

right to left in the anterior region of KV (Kramer-Zucker et al., 2005; Kreiling et al., 2007; Okabe et al., 2008). Asymmetric placement of LR ciliated cells provides a potential mechanism for aligning the embryonic axes, but pathways that control positioning of cells in KV have not been previously identified.

We hypothesized that Rho GTPase signaling is involved in establishing the asymmetric architecture of KV. Rho GTPases signal through the Rho-associated coiled-coil containing protein kinase (Rock) proteins, Rock1 or Rock2, to modulate cytoskeletal dynamics and intracellular signaling to control several cellular processes including motility, morphology and adhesion (Noma et al., 2006). Several lines of evidence implicate Rho GTPase signaling in LR development, but mechanisms have not been elucidated. In zebrafish, antisense morpholino oligonucleotide (MO) knockdown of *arhgef-11*, a Rho guanine nucleotide exchange factor (RhoGEF), alters asymmetric *nodal* expression in LPM and disrupts heart and gut laterality (Panizzi et al., 2007). In the chick embryo, antisense knockdown of Rock1 or Rock2 results in heart development defects, including defects in LR asymmetric looping of the heart tube (Wei et al., 2001). Mouse and chick embryos treated with a small molecule inhibitor of Rho kinase, Y-27632, develop heart defects (Wei et al., 2001), and treated chick embryos show bilateral *nodal* expression in LPM. Based on these studies, we predicted that a zebrafish Rho kinase gene, *rock2b*, that is expressed in KV (Thisse et al., 2001) might regulate KV architecture and subsequent LR development.

Here, we show Rock2b is required for the asymmetric placement of LR ciliated cells along the AP axis in KV. In wild-type embryos, a dense accumulation of ciliated cells in the anterior region of KV correlates with strong right-to-left fluid flow. Depletion of *rock2b* disrupts the AP asymmetric architecture of KV, abrogates fluid flow in KV and alters asymmetric gene expression in LPM and organ laterality. Furthermore, we show *rock2b* plays a cell-autonomous role in DFC/KV cells to control LR development. Live imaging of transgenic embryos that express membrane localized green fluorescent proteins (GFP) in KV cells revealed that *rock2b* knockdown alters KV cell morphology. These results identify the first gene involved in establishing AP asymmetry of KV, and suggest a link between AP and LR patterning in the ciliated KV.

MATERIALS AND METHODS

Zebrafish

Wild-type AB zebrafish (*Danio rerio*) were obtained from the Zebrafish International Resource Center (ZIRC). Embryos collected from natural matings were cultured using standard protocols (Westerfield, 1995) and staged according to Kimmel et al. (Kimmel et al., 1995).

Embryo injections

MO designed to block *rock2b* RNA splicing (*rock2b* MO-1; 5′-GCACACACTCACTCACCAGCTGCAC-3′) or translation (*rock2b* MO-2; 5′-CATTGCGGCAGCTCGGTGTCCTTAA-3′) and a standard negative control MO (5′-CCTCTTACCTCAGTTACAATTTATA-3′) were obtained from Gene Tools, LLC. To deliver MO to all embryonic cells, embryos were injected at the 1- to 4-cell stages (Nasevicius and Ekker, 2000) with 0.4 ng *rock2b* MO-1, 4.4 ng *rock2b* MO-2 or 4.4 ng control MO (unless otherwise noted). To generate DFC^{MO} embryos, we co-injected 0.8 ng *rock2b* MO-1 with 2.6 ng fluorescent-tagged control MO, 4.4 ng *rock2b* MO-2 or 4.4 ng control MO into the yolk cell at ~1000-cell stage, and then selected embryos in which fluorescent MO diffused throughout the yolk and entered DFC/KV cells for analysis (Amack and Yost, 2004). To generate yolk^{MO} embryos, we injected MO into the yolk cell between the dome stage and 30% epiboly stage. For RT-PCR analysis of *rock2b* MO-1 efficacy, total RNA was isolated using Trizol (Invitrogen) and cDNA was synthesized using the Ambion Retroscript kit. cDNA was amplified using *rock2b* and β-actin primers that are available upon request. For DNA injections, 20 ng of plasmid encoding dominant negative Rho kinase (DN-Rock) (Ishizaki et al., 1997) or control yellow fluorescent protein (pEYFP-N1) were injected at the one-cell stage. DN-Rock is p160ROCK harboring a point mutation that changes amino acid 105 from lysine to alanine and disrupts the kinase domain. Expression of both DN-Rock and EYFP were driven by a cytomegalovirus (CMV) promoter.

rock2b cloning and mRNA rescue

The cb64 cDNA clone, which contains a partial open reading frame of *rock2b*, was obtained from ZIRC. We cloned the full-length cDNA using nested PCR (PFUltra, Stratagene) from a reverse transcribed early zebrafish RNA pool (Ambion Retroscript). Primers are available upon request. The resulting PCR product (~4.2 kb) was inserted into pCR4-Blunt Topo (Invitrogen). The full-length sequence can be obtained from GenBank (GQ395807). A *rock2b* mRNA expression plasmid was created by inserting the open reading frame (*Pci*I-*Xba*I fragment) into a pCS-2 vector containing *Nco*I and *Xba*I sites. For rescue experiments, the mMessage mMachine kit (Ambion) was used to synthesize capped mRNA from the *rock2b* plasmid or a constitutively active Rock (CA-Rock) construct, previously characterized as pCAG-myc-p160Δ3 (Ishizaki et al., 1997), which has the regulatory Rho-binding domain deleted. The resulting mRNA was diluted and injected as above.

RNA in situ hybridization

RNA probes were labeled with digoxygenenin (Roche DIG RNA labeling kit) to detect *rock2b*, *shh* (Krauss et al., 1993), *cmlc2* (*myl7* – Zebrafish Information Network) (Yelon et al., 1999), *foxa3* (Odenthal and Nusslein-Volhard, 1998), *spaw* (Long et al., 2003) and *charon* (Hashimoto et al., 2004). In situ hybridizations were performed as described (Essner et al., 2000). For sectioning, embryos were embedded in gelatin/albumin solution as described (Albertson et al., 2010) and sectioned at 35 μm using a Vibrotome 1500.

Fluorescent immunostaining

Whole-mount fluorescent immunostaining was performed as described (Amack et al., 2007). Primary antibodies used were mouse anti-acetylated tubulin (1:400, Sigma) and rabbit anti-aPKC (1:200, Santa Cruz). Secondary antibodies were Alexa Fluor 488-conjugated anti-mouse IgG (1:200, Invitrogen) and Alexa Fluor 647-conjugated anti-rabbit IgG (1:200, Invitrogen). Alexa Fluor 568-conjugated phalloidin (1:200, Invitrogen) was added with secondary antibodies. For imaging, whole embryos were mounted in 1% low melting agarose and analyzed using a 63× water dipping objective on a Zeiss Imager M1 AX10 microscope. Images were captured with a Zeiss Axiocam HSm digital camera and processed using AxioVision software (Zeiss). To analyze cilia number, length and AP distribution we used Z-projections of the entire KV generated using ImageJ software (NIH). To bisect KV into anterior and posterior regions, a line was first drawn extending from the notochord across KV and a second line was drawn perpendicular to the first line at the midpoint to along the AP axis. *P* values were calculated using the Student's t-test.

KV fluid flow and cilia motility

Fluorescent beads (Polysciences) were injected into KV to visualize flow as described (Essner et al., 2005). Bead flow and cilia beating were imaged at the 8- to 10-somite stage (SS) on either a Leica DMRA microscope using a 40× Plan Apo objective and a coolsnap HQ camera (Photometrics) or a Zeiss Imager M1 AX10 microscope using a 63× water dipping objective and a Zeiss Axiocam HSm high speed camera. Movies were generated using Metamorph (Universal Imaging), Axiovision (Zeiss) and Quicktime (Apple) software. Metamorph and Axiovision were used to track individual beads and calculate velocity. A differential interference contrast (DIC) image was used to divide KV into quadrants by drawing a line extending from the notochord to establish left and right sides and a second perpendicular line at the midpoint to delineate the AP boundary. For each embryo, four to five beads were tracked for a minimum of 50 frames of the movie and the average bead velocity was calculated for each quadrant. Axiovision was also used to measure the size of KV in DIC images. The percentage of cilia showing abnormal motility was determined by blind scoring of DIC movies.

Generation of transgenic *Tg(Dusp6:memGFP)* zebrafish

Tg(dusp6:memGFP) lines were generated as previously described (Molina et al., 2007). Briefly, the *dusp6* promoter, a 10 kb Kpn1 fragment containing parts of Exon 1 (441 bp) and approximately 9.5 kb of upstream promoter sequence was subcloned into the *Kpn*I site of pSceImemGFP vector (Zernicka-Goetz et al., 1996). Twenty picograms of *pdusp6:memGFP* plasmid DNA was injected into the one-cell embryo with I-*Sce*I (New England Biolabs) restriction enzyme as described in Thermes et al. (Thermes et al., 2002). Injected embryos were raised to adulthood and we identified several founder lines that expressed memGFP in a similar manner as *Tg(dusp6:EGFP)*^{pt6} (Molina et al., 2007). *Tg(dusp6:memGFP)*^{pt19} embryos exhibited strong expression throughout development and were used in this study.

Imaging and cell shape analysis of fluorescent KV cells in live embryos

At 8-SS, *Tg(dusp6:memGFP)*^{pt19} embryos were dechorionated and immobilized in 1% low melting agarose on a MetTek dish (MetTek). Images were obtained using a Perkin-Elmer Ultra VIEW Vox spinning disc confocal microscope. Z-series images of KV cells were collected every minute for 1 hour. Recordings were analyzed using Volocity 5.3.0 and ImageJ software. To analyze length-width ratio (LWR) of KV cells, the middle focal plane (with the largest KV lumen diameter) was chosen. Cell length and cell apical width were measured using ImageJ.

RESULTS

The arrangement of ciliated cells in KV is asymmetric along the AP axis

We hypothesize that the relative position of LR ciliated cells in the embryo mediates the alignment of the LR axis with the previously established DV and AP axes. To characterize the arrangement of cells in KV, we performed fluorescent immunostaining experiments using acetylated tubulin antibodies to label LR cilia and atypical Protein Kinase C (aPKC) antibodies to mark apical membranes of KV cells (Fig. 1A). Shown in Fig. 1A,B is the dorsal surface of KV, where the majority of cilia are located (Kreiling et al., 2007; Okabe et al., 2008). When all cilia were counted in wild-type embryos at the 8-SS, we found an average distribution of 63% of cilia positioned in the anterior half of KV and 37% positioned in the posterior region (Fig. 1B). This AP asymmetry of LR cilia was consistent with previous reports (Kreiling et al., 2007; Okabe et al., 2008). In addition, aPKC staining showed that cells in the posterior region of KV had large apical surfaces (arrowhead in Fig. 1A), whereas cells in the anterior region had smaller apical surfaces (arrow in Fig. 1A), which may facilitate the packing of more ciliated cells into the anterior region (Okabe et al., 2008). These analyses indicated that the AP asymmetric arrangement of LR ciliated cells is associated with differences in cell morphology.

Strong right-to-left asymmetric fluid flow in the anterior region of KV

Counterclockwise fluid flow in KV is from right to left at the anterior pole and from left to right at the posterior end. It is unknown how this flow establishes biological LR asymmetries. It has been reported that flow is stronger from right to left (Kramer-Zucker et al., 2005; Kreiling et al., 2007; Okabe et al., 2008), analogous to net leftward flow in the mouse node. However, regional flow has not been quantified in KV. To address this, we injected fluorescent beads into KV at 8- to 10-SS (Essner et al., 2005) and analyzed flow velocity. In wild-type embryos, beads indeed appeared to move faster from right to left at the anterior end (see Movie 1 in the supplementary material). We tracked individual beads (Fig. 1C) and calculated the average bead velocity in different quadrants of KV. This analysis revealed regional differences in the velocity of flow produced in KV (Fig. 1D). The highest velocities and most variability were observed in the anterior quadrants of KV (Fig. 1D). Flow was slower and more consistent in posterior quadrants (Fig. 1D). This was the first quantitative analysis of flow velocity that supports a model in which a dense population of ciliated cells drives strong right-to-left flow across the anterior region of KV and fewer ciliated cells generate a weaker return flow in the posterior region.

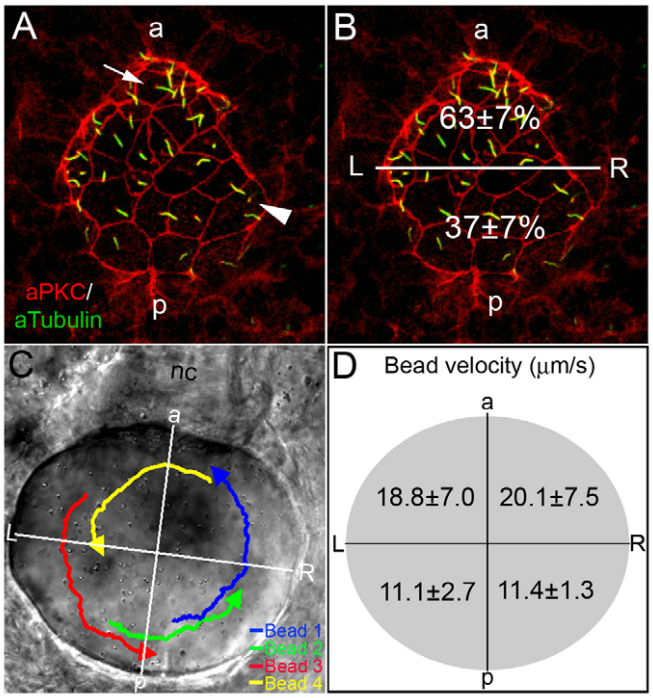

Fig. 1. AP asymmetry in KV. (**A**,**B**) Fluorescent immunostaining of KV cells at 8-SS with aPKC (red) and acetylated tubulin (green) antibodies. To visualize individual cells, only the dorsal surface of KV is shown. Cells in the posterior region of KV had large apical surfaces (arrowhead), whereas cells in the anterior region had smaller apical surfaces (arrow). Counting all KV cilia in wild-type embryos (n=13), revealed a significant difference (P=3.60E-5) in the positioning of cilia with 63% located in the anterior half of KV and 37% are in the posterior region (B). (**C**,**D**) Tracking fluorescent beads injected into KV shows fluid flow velocity is asymmetric. (C) Paths of beads and the AP and LR axes of KV, relative to the notochord, have been superimposed onto a DIC image of KV. (D) The average velocity of 23 beads from 5 wild-type embryos in quadrants of KV indicated that flow was significantly stronger from right to left in the anterior region than in the posterior of KV (P<0.05). Numbers are averages ± one s.d. L, left; R, right; a, anterior; p, posterior; nc, notochord.

rock2b is expressed in the DFC/KV cell lineage

A large scale RNA in situ hybridization screen in zebrafish identified a Rho kinase gene, *rock2b*, which was strongly expressed in KV (Thisse et al., 2001). Based on previous studies implicating Rho-Rho kinase signaling in LR development (Panizzi et al., 2007; Wei et al., 2001), we postulated Rock2b may play a role in the form or function of KV. To further characterize the expression profile of *rock2b*, we obtained a partial *rock2b* cDNA probe (cb64) and cloned a cDNA fragment from the 3′ end of the gene and conducted RNA in situ hybridizations. We observed strong *rock2b* RNA expression in surface epithelial enveloping layer (EVL) cells,

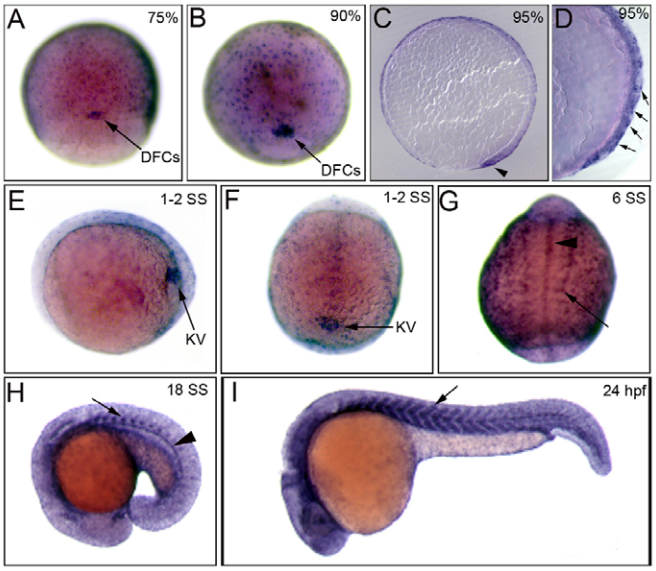

Fig. 2. *rock2b* is expressed in the DFC/KV cell lineage. (**A**,**B**) Whole embryo RNA in situ hybridization staining shows *rock2b* is expressed in DFCs (arrows) and the enveloping layer at 75% (A), 90% epiboly (B). (**C**,**D**) Sagittal sections of stained embryos at 95% epiboly show *rock2b* expression in DFCs (arrowhead) and the EVL (arrows). (**E**,**F**) During early SSs, *rock2b* is detected in KV cells (arrow). (E) is a lateral view at 1- to 2-SS and (F) is a dorsal view. (**G-I**) During later somitogenesis, *rock2b* is expressed in somites (arrows) and midline structures including the hypochord and notochord (arrowheads).

DFCs and KV cells (Fig. 2A-F). We also detected *rock2b* expression in somites and midline structures including the hypochord and notochord during later SSs (Fig. 2G-I). After 24 hours postfertilization (hpf), *rock2b* was expressed primarily in the brain and midline (data not shown). *rock2b* expression was not observed in the yolk cell or other ciliated tissues, such as the pronephric ducts or otic vesicles. The robust expression of *rock2b* in DFC/KV cell lineage made *rock2b* a strong candidate gene for regulating KV morphogenesis.

Rock2b is required for normal LR development

To determine whether *rock2b* is required for LR development in zebrafish we designed a MO to interfere with RNA splicing and knockdown Rock2b protein expression. Embryos injected with this MO (*rock2b* MO-1) showed dose-dependent defects (see Fig. S1B,C in the supplementary material), including axis elongation defects reminiscent of abnormal convergent and extension (CE) in zebrafish embryos expressing dominant-negative Rho kinase proteins (Marlow et al., 2002). RT-PCR analysis of *rock2b* mRNA in embryos injected with *rock2b* MO-1 revealed a dose-dependent reduction of normally spliced *rock2b* mRNA (see Fig. S1D in the supplementary material). A low MO dose (0.4 ng) that resulted in partial depletion of *rock2b* mRNA (see Fig. S1D in the supplementary material) and had little or no effect on axis elongation (Fig. 3A,B) was chosen for subsequent experiments.

We first assessed organ laterality at 48 hpf by RNA in situ hybridization using the heart marker *cmlc2* (Fig. 3C-E) and gut marker *foxa3* (Fig. 3F-H). Wild-type and control MO-injected embryos showed normal rightward heart looping (Fig. 3C,I; see Table S1 in the supplementary material) and normal asymmetric orientation of the liver and pancreas (Fig. 3F,I; see Table S1 in the

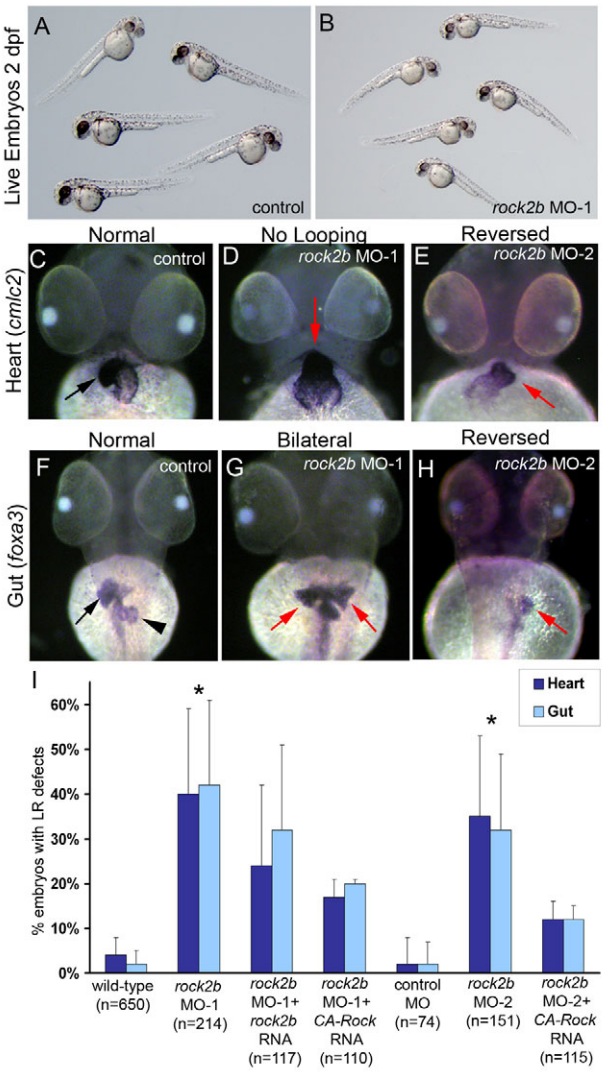

Fig. 3. *rock2b* knockdown alters heart and gut laterality. (**A**,**B**) Embryos injected with a low dose of *rock2b* MO-1 (B) appeared similar to wild-type controls (A) at 2 dpf, (**C-E**) Analysis of heart looping at 2 dpf by *cmlc2* RNA in situ hybridizations revealed normal rightward looping in control embryos (arrow in C), and LR defects including a failure of heart looping (arrow in D) and reversed looping (arrow in E) in *rock2b* MO embryos. (**F-H**) *foxa3* was used to label liver (arrow) and pancreas (arrowhead) at 2 dpf. Controls showed normal asymmetric orientation of these organs (F), whereas they were often bilaterally symmetric (arrows in G) or in a reversed position (arrow in H) in *rock2b* MO embryos. (**I**) The percentage of embryos injected with MO or MO + rescue mRNA which showed heart and gut laterality defects are presented in the graph and in Table S1 in the supplementary material. *Significantly different (P<0.05) from wild-type and control MO embryos. Error bars indicate +1 s.d. n=number of embryos analyzed.

supplementary material). By contrast, the heart and gut were frequently bilaterally symmetric (Fig. 3D,G) or reversed (Fig. 3E,H) in *rock2b* MO-injected embryos (Fig. 3I; see Table S1 in the supplementary material). To test whether LR defects were specific to *rock2b* knockdown, we performed rescue experiments in which *rock2b* mRNA was co-injected with *rock2b* MO-1. We observed a dose-dependent partial rescue of LR defects in the heart and gut (Fig. 3I; see Table S1 in the supplementary material). Higher doses of *rock2b* mRNA resulted in severe defects during

gastrulation. Injection of control GFP mRNA did not ameliorate *rock2b* MO-1 phenotypes (see Table S1 in the supplementary material). As a second approach, we co-injected *rock2b* MO-1 with mRNA encoding a previously characterized (Ishizaki et al., 1997) constitutively active Rho kinase (CA-Rock). Expression of CA-Rock also partially rescued *rock2b* MO-1 laterality defects (Fig. 3I; see Table S1 in the supplementary material). To further test the specificity of *rock2b* MO phenotypes, we designed a second MO (*rock2b* MO-2) to block *rock2b* translation. Similar to *rock2b* MO-1, *rock2b* MO-2 caused variable dose-dependent axis elongation defects (see Fig. S1F,G in the supplementary material) and heart and gut laterality defects (Fig. 3E,H,I; see Table S1 in the supplementary material). These laterality defects were also reduced by co-injection of *CA-Rock* mRNA in two out of three experiments (Fig. 3I; see Table S1 in the supplementary material). Taken together, similar phenotypes using two different MOs and rescue of MO phenotypes by co-expression of wild-type Rock2b or CA-Rock indicated that LR defects are specific to *rock2b* knockdown.

In zebrafish, the first asymmetrically expressed gene in LPM is the *nodal*-related gene *southpaw* (*spaw*) (Long et al., 2003), which encodes a component of the conserved Nodal-Lefty-Pitx2 signaling cascade. RNA in situ hybridizations revealed that in contrast to normal left-sided expression in controls (Fig. 4A,D), *spaw* expression was frequently aberrant in *rock2b* MO embryos (Fig. 4B-D). In affected embryos, *spaw* expression was predominantly bilateral, although we observed embryos with right-sided or absent expression (Fig. 4D). Bilateral *nodal*/*spaw* expression can result from defects in the embryonic midline (Chen et al., 1997; Danos and Yost, 1995; Danos and Yost, 1996; Meno et al., 1998). However, midline structures appeared normal in *rock2b* knockdown embryos as visualized by brightfield microscopy (see Fig. S2A,E in the supplementary material) and by the expression of the midline markers *sonic hedgehog* (*shh*) (see Fig. S2B,C,F,G in the supplementary material) and *no tail* (*ntl*) (see Fig. S2D,H in the supplementary material). These results were consistent with a function for Rock2b in KV upstream of asymmetric *spaw* expression and independent of midline formation.

As an alternative approach to test whether LR development in zebrafish depends on Rho kinase function, we expressed dominant negative Rho kinase (DN-Rock) proteins (Ishizaki et al., 1997) in embryos. DN-Rock expression has previously been shown to increase mesoderm induction (Zhang et al., 2009) and cause CE defects during gastrulation, including axis elongation defects (Marlow et al., 2002). These abnormalities make it difficult to interpret the role of Rock activity at later developmental stages. To avoid severe early phenotypes, we injected DNA constructs to facilitate later and more mosaic expression of DN-Rock proteins. The majority of embryos injected with 20 pg of DNA encoding DN-Rock (75%, *n*=70) showed normal axis elongation at 2 days postfertilization, whereas 16% developed mild axial defects and 9% developed severe axis elongation defects (see Fig. S3A,B in the supplementary material). These embryos showed a high incidence of bilateral *spaw* expression (Fig. 4D; see Fig. S3D in the supplementary material) and altered heart looping (see Fig. S3E-H in the supplementary material), reminiscent of *rock2b* morphant embryos. LR defects were not observed in embryos injected with control DNA encoding yellow fluorescent proteins (YFP) (Fig. 4D; see Fig. S3C,E,H in the supplementary material). Taken together, *rock2b* MO knockdowns and expression of DN-Rock proteins indicated that Rho kinase signaling is required during an early step in zebrafish LR development to regulate *spaw* asymmetry.

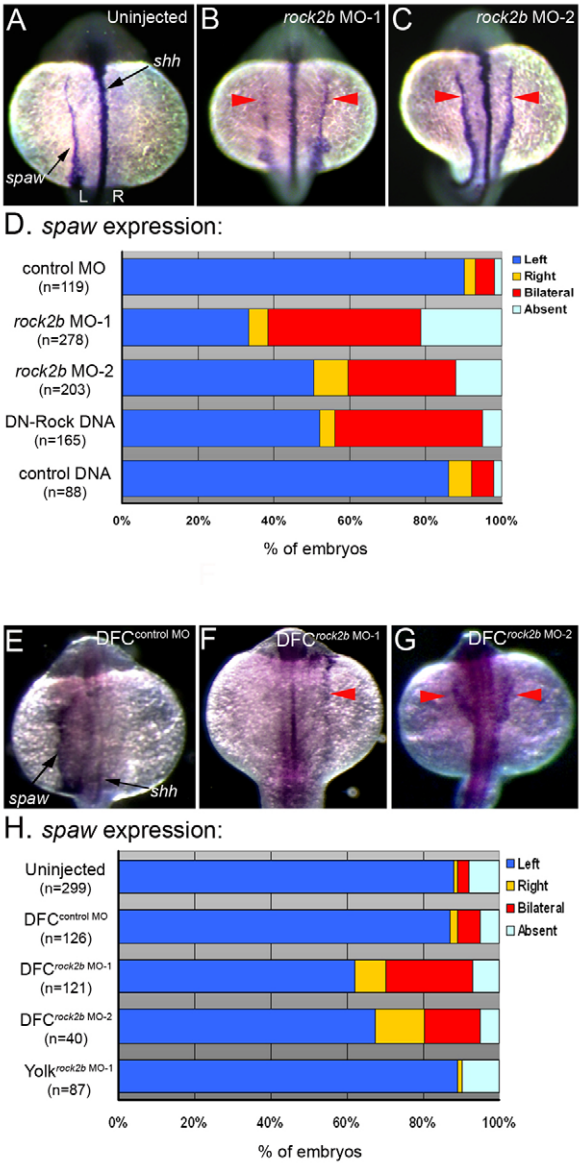

Fig. 4. Rock2b function in DFC/KV cells is required for normal asymmetric *southpaw* expression. (**A-C**) *spaw* is normally expressed in left LPM in control embryos (A) at 16- to 18-SS. In contrast, *spaw* expression was often bilateral in *rock2b* MO embryos (red arrows in B,C). *shh* expression (see arrow in A) indicated that embryonic midline structures were intact. (**D**) The frequency of altered *spaw* expression (right, bilateral or absent) in control embryos and embryos injected with *rock2b* MO or DNA encoding DN-Rock proteins. (**E-G**) *spaw* expression was altered in DFC$^{rock2b\ MO}$ embryos (F,G), whereas normal left-sided expression was observed in most control DFC$^{control\ MO}$ embryos (E). (**H**) The percentage of DFC$^{rock2b\ MO}$ and control embryos with *spaw* defects. *n*=number of embryos analyzed.

Rock2b functions in the DFC/KV cell lineage to control LR asymmetry

Consistent with our results in zebrafish, inhibition of Rho kinase has been shown to alter LR development in chick and mouse embryos (Wei et al., 2001). However, the developmental stages and embryonic locations of Rho kinase function for LR development are unknown. To directly test whether Rock2b functions in LR ciliated cells, we delivered *rock2b* MO exclusively to the DFC/KV

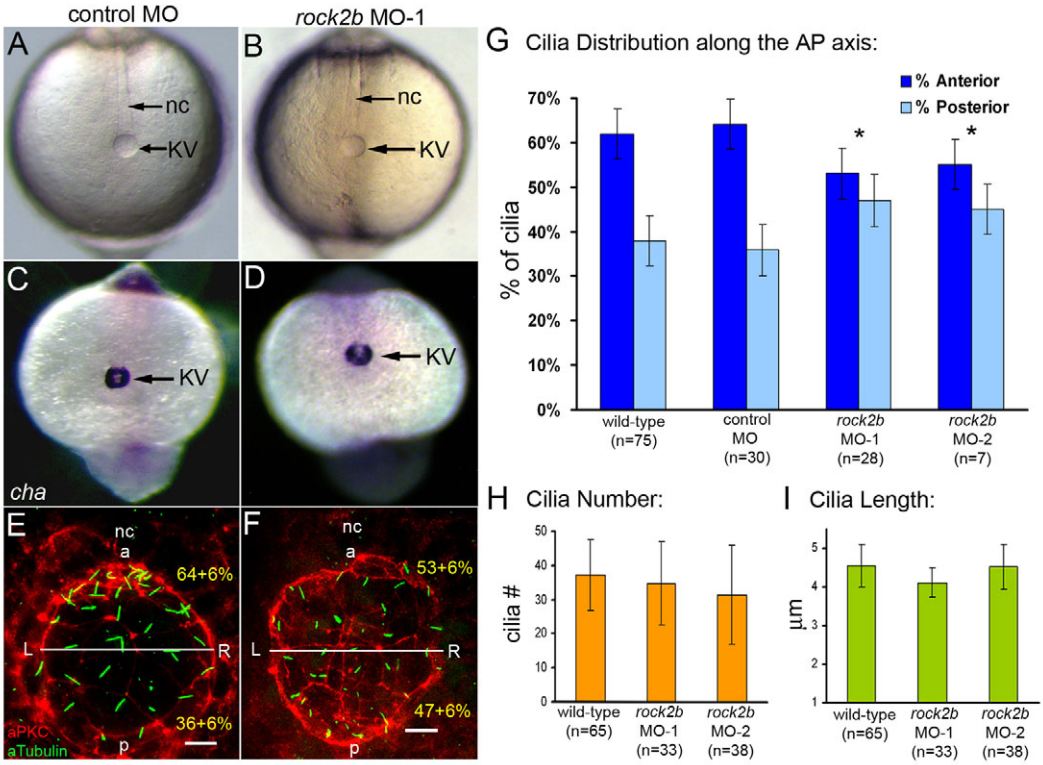

Fig. 5. *rock2b* knockdown disrupts AP asymmetric arrangement of KV cilia without inhibiting KV lumen formation or ciliogenesis. (**A**,**B**) Light micrographs at 8-SS show KV lumen (arrow) appeared similar in control MO (A) and *rock2b* MO (B) embryos. Surrounding tailbud tissue and nc also appeared similar. (**C**,**D**) Normal *cha* expression around KV (arrow) in control MO (C) and *rock2b* MO (D) embryos at 10- to 12-SS. (**E**,**F**) Fluorescent immunostaining of KV using aPKC and acetylated tubulin antibodies in control MO (E) and *rock2b* MO (F) embryos at 8-SS. KV was bisected into anterior and posterior regions using the position of the nc. (**G**) The average AP distribution ± 1 s.d. is shown (also shown in yellow in E and F). *The AP distribution of ciliated cells was significantly different ($P<0.01$) from controls. (**H**,**I**). There were no statistical differences ($P>0.05$) in cilia number or length among wild-type (37±10 cilia; 4.5±0.5 μm), *rock2b* MO-1 (34±12 cilia; 4.1±0.4 μm) and *rock2b* MO-2 (32±15 cilia; 4.5±0.6 μm) embryos. Scale bars: 10 μm. Error bars: 1 s.d. nc, notochord; a, anterior; p, posterior; L, left; R, right. *n*=number of embryos analyzed.

cell lineage (Amack et al., 2007; Amack and Yost, 2004). This approach creates embryos (referred to as DFC$^{rock2b\ MO}$ embryos) in which *rock2b* is knocked down in DFC/KV cells, but remains normal in other embryonic cells. Similar to global interference of Rho kinase signaling by *rock2b* MO or DN-Rock, DFC$^{rock2b\ MO\text{-}1}$ and DFC$^{rock2b\ MO\text{-}2}$ embryos developed *spaw* LR defects (Fig. 4H), including right-sided (Fig. 4F) and bilateral (Fig. 4G) expression, which were not observed in DFC$^{control\ MO}$ embryos (Fig. 4E,H). As an important control (Amack et al., 2007; Amack and Yost, 2004), we tested whether LR defects in DFC$^{rock2b\ MO}$ embryos were due to MO activity in the yolk cell rather than DFC/KV cells. In these experiments, MO was restricted to the yolk cell to generate yolk$^{rock2b\ MO}$ embryos. LR defects seen in DFC$^{rock2b\ MO}$ embryos were not seen in yolk$^{rock2b\ MO}$ embryos (Fig. 4H). These results identified a role for Rho kinase signaling in the DFC/KV cell lineage during LR development.

Rock2b is required for establishing an AP asymmetric arrangement of LR ciliated cells in KV

LR patterning in zebrafish is dependent on normal KV morphogenesis, which includes formation of the KV lumen (Amack et al., 2007; Amack and Yost, 2004). By light microscopy, the KV lumen appeared normal at 8-SS in *rock2b* MO-1 (Fig. 5B; *n*=90/93) and *rock2b* MO-2 (*n*=50/52) embryos, similar to control MO embryos (Fig. 5A; *n*=97/106). Measurements of the area of KV indicated no significant differences in lumen size among wild-type (3090±569 μm^2, *n*=7), *rock2b* MO-1 (3361±715 μm^2, *n*=10) and *rock2b* MO-2 (3213±1149 μm^2, *n*=8) embryos. Consistent with these results, expression of *charon* (*cha*), a nodal-signaling antagonist required for asymmetric *spaw* expression (Hashimoto et al., 2004), appeared normal in cells surrounding KV at 10- to 12-SS in control MO (Fig. 5C; *n*=25/26) and *rock2b* MO-1 (Fig. 5D; *n*=80/83) embryos. Thus, specification of cells in and around KV in the tailbud and formation of the KV lumen appeared to be unaffected by *rock2b* knockdown.

To analyze the distribution of ciliated cells along the AP axis in KV, we double-labeled KV cells at 8-SS with acetylated tubulin and aPKC antibodies. Similar to wild-type embryos (Fig. 1B), control MO embryos had an average of 64±6% of cilia positioned in the anterior half of KV and 36±6% in the posterior half (Fig. 5E,G). This AP asymmetry was disrupted in *rock2b* MO-1 knockdown embryos, in which 53±6% of KV cilia were in the anterior region and 47±6% of cilia were in the posterior region (Fig. 5F,G). A similar loss of AP asymmetry was observed in KVs of *rock2b* MO-2 embryos (Fig. 5G). Importantly, the average number (Fig. 5H) and length (Fig. 5I) of KV cilia was not significantly different between wild-type and *rock2b* MO embryos. Taken together, our results show *rock2b* regulates AP asymmetry of cilia distribution in KV without inhibiting lumen formation or altering cilia number or length.

Rock2b is necessary for asymmetric flow in KV

We next tested whether the altered AP arrangement of KV ciliated cells in *rock2b* MO embryos altered fluid flow. Fluorescent beads injected into the KV lumen of wild-type (see Movie 1 in the supplementary material) and control MO embryos flowed in a counterclockwise direction. By contrast, beads moved about randomly in *rock2b* MO-1 embryos (see Movie 2 in the supplementary material) and *rock2b* MO-2 embryos (data not shown), indicating a loss of coordinated flow. Tracking beads in KV showed counterclockwise directional paths in control MO embryos (Fig. 6A), but this directionality was lost in *rock2b* MO embryos (Fig. 6C). In addition, beads tracked in *rock2b* MO embryos showed a reduced average flow velocity relative to controls (Fig. 6E). When flow was analyzed in different quadrants of KV, beads in control MO embryos showed higher velocities in the anterior end (Fig. 6B). By contrast, beads tracked in *rock2b* MO embryos showed similar velocities in all quadrants (Fig. 6D), indicating a loss of regional asymmetric flow.

DIC videomicroscopy revealed that the majority of cilia in *rock2b* MO-1 embryos (78%; *n*=73 cilia from 14 embryos) showed normal rotational beating (green arrows in Movie 3 in the supplementary material) which was similar to most cilia in control MO embryos (96%; *n*=48 cilia from 10 embryos). However, some cilia (22%) in *rock2b* MO-1 embryos showed abnormal beating (red arrow in Movie 3 in the supplementary material). In addition, we observed cilia that appeared to interfere with one another (yellow arrow in Movie 3 in the supplementary material) in several *rock2b* MO-1 embryos (*n*=8/14), probably owing to the altered arrangement of cilia in KV. We next visualized cilia in KVs injected with fluorescent beads. In control embryos, we observed beating cilia and counterclockwise flow of beads (data not shown). In *rock2b* MO-1 embryos, cilia that showed normal beating (red arrows in Movie 4 in the supplementary material) failed to generate a directional flow, resulting in random movement of beads (see Movie 4 in the supplementary material). These analyses suggest Rock2b-mediated positioning of KV cilia is necessary for producing coordinated flow in KV.

Rock2b controls morphology of LR ciliated cells in KV

Rho kinase can phosphorylate several substrates; many of these control actin-myosin assembly, stability or contractility (reviewed in Riento and Ridley, 2003). Therefore, we analyzed actin structures in KV cells of *rock2b* MO embryos by double immunofluorescence labeling of apical membranes with aPKC antibodies and filamentous actin with phalloidin. aPKC localized to the apical surface of KV cells in both control (Fig. 7A) and *rock2b* MO (Fig. 7D) embryos, indicating normal apicobasal polarity. Furthermore, we observed apical actin structures in KV cells (Oishi et al., 2006) that appeared similar in both control (Fig. 7B,C) and *rock2b* MO (Fig. 7E,F) embryos. However, these experiments revealed abnormal KV cell morphologies in *rock2b* MO embryos. Compared with control embryos, more KV cells in *rock2b* MO embryos appeared to have large apical surfaces (compare Fig. 7C and 7F). This suggested that *rock2b* MO knockdown does not affect assembly or localization of apical actin structures, but rather alters KV cell shape.

To further characterize KV cell morphology in *rock2*b MO embryos, we imaged live transgenic *Tg*(*dusp6:memGFP*)^{pt19} embryos that express cell-membrane-localized green fluorescent proteins (memGFP) in KV cells. In these embryos memGFP expression is driven by the *dual specificity phosphatase 6* (*dusp6*)

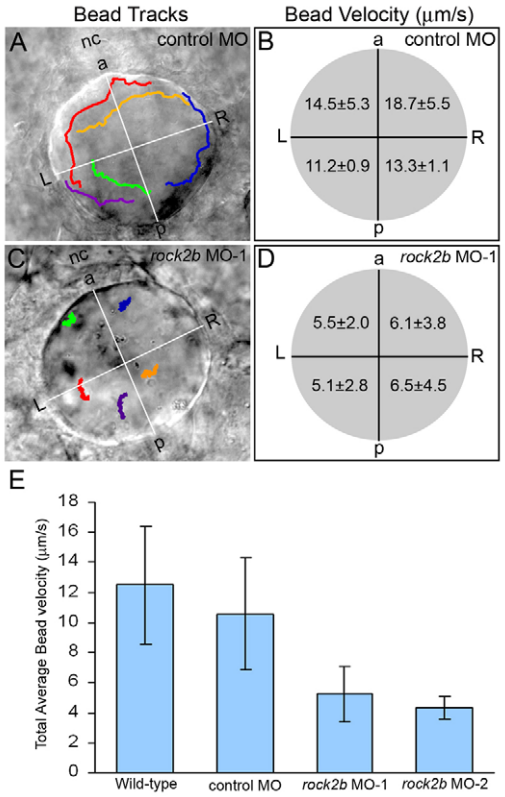

Fig. 6. Asymmetric KV fluid flow is disrupted by *rock2b* knockdown. (**A**,**C**) Tracks of fluorescent beads superimposed on DIC images of KV. Beads followed a counterclockwise path in control MO embryos (A), but this directional flow was lost in *rock2b* MO embryos (C). (**B**,**D**) Measurements of bead velocities in quadrants of KV showed that flow was stronger in the anterior region of control MO embryos (B; *n*=28 beads from six embryos), but velocities were similar in all quadrants of r*ock2b* MO embryos (D; *n*=30 beads from seven embryos). (**E**) Total average flow velocity was reduced in *rock2b* MO embryos relative to controls. Average velocity is shown for uninjected (*n*=35 beads from seven embryos), control MO (*n*=30 beads from six embryos), *rock2b* MO-1 (*n*=70 beads from 14 embryos) and *rock2b* MO-2 (*n*=19 beads from four embryos) embryos. Error bar: 1 s.d. nc, notochord; a, anterior; p, posterior; L, left; R, right.

promoter in response to FGF signaling (Molina et al., 2007). Membrane localization of GFP in KV provides a clear distinction of cell borders, membrane protrusions and cell shapes, facilitating analyses of cell behavior and morphology. Live imaging at 8-SS showed that KV cells in control MO embryos were dynamic, and extended and retracted membrane protrusions (see Movie 5 in the supplementary material). KV cells in the anterior region were long and narrow with small apical surfaces, whereas posterior KV cells were short and wide and had large apical size (see Movie 5 in the supplementary material), consistent with our immunostaining results (Fig. 1A). By contrast, KV cells in *rock2b* MO-1 and DFC$^{rock2b\ MO\text{-}1}$ embryos were irregularly shaped and did not show the distinct anterior and posterior morphologies seen in controls (see Movies 6 and 7 in the supplementary material). Importantly, *dusp6:memGFP* embryos revealed defects in KV structure that were not apparent by light microscopy (see Fig. 5A,B and Fig. 6A,C). To quantify differences in cell morphology, we analyzed optical sections through the middle focal plane of KV at 8-SS (Fig.

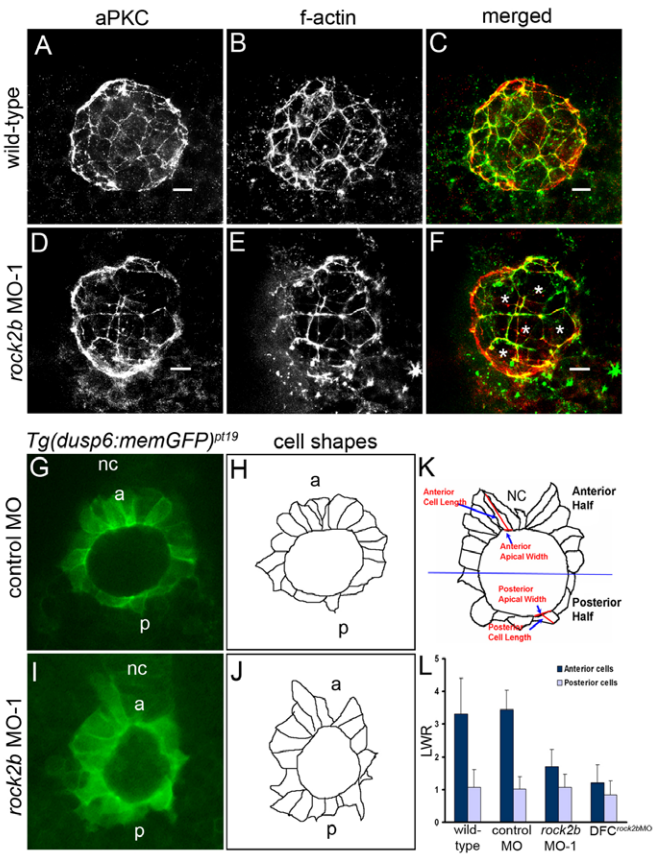

Fig. 7. rock2b knockdown alters KV cell shapes. (**A-F**) KV cells at 8-SS double fluorescently labeled with aPKC antibodies (A,D) and phalloidin (B,E) to detect apical membrane and filamentous actin (f-actin), respectively. Apical actin structures were present and co-localized with aPKC similarly in wild-type (A-C) and *rock2b* MO-1 (D-F) embryos, but the architecture of KV appeared different in *rock2b* MO-1 embryos, in which more KV cells had large apical surfaces (examples are marked by * in F). (**G**,**I**) Confocal images of memGFP-labeled KV cells in live Tg(*d*usp6:*m*emGFP)^{pt19} transgenic embryos injected with control MO (G) or rock2b MO-1 (I). (**H**,**J**) Diagrams show KV cell shapes traced from confocal images. (**K**) Diagram of KV cells in a wild-type embryo, with a description of how the LWR was measured in anterior and posterior KV cells. (**L**) The average LWR for wild-type (*n*=12 embryos) control MO (*n*=5) and rock2b MO-1 (*n*=15) and DFC$^{rock2b\ MO\text{-}1}$ (*n*=4) embryos. Scale bars: 10 μm. Error bars: 1 s.d. nc, notochord; a, anterior; p, posterior.

7G-J) and calculated the LWR of cells in the anterior and posterior regions (Fig. 7K). In controls, the LWR of anterior cells was significantly different than posterior cells (Fig. 7L). However, in *rock2b* MO and DFC$^{rock2b\ MO\text{-}1}$ embryos, cell morphologies were similar in both the anterior and posterior regions (Fig. 7L). Thus, Rock2b plays a cell-autonomous role controlling KV architecture by regulating KV cell morphology.

DISCUSSION

Asymmetric fluid flow generated by ciliated cells at the node in mouse, notochordal plate in rabbit, gastrocoel roof plate in frog, and KV in medaka and zebrafish has been implicated in LR development, indicating a conserved role for specialized ciliated epithelia in LR axis formation. As the embryonic location and cellular architecture of these apparently analogous epithelia differs among species, we propose unifying terms to avoid confusing nomenclature: we refer to the transient cilia that generate fluid flow as 'LR cilia' and the cilia-driven fluid flow as 'asymmetric flow.' Here, we report a Rho kinase gene that controls the placement of LR cilia along the AP axis of KV and is necessary for asymmetric flow. We demonstrate that *rock2b* regulates KV architecture by modulating cell shapes. *rock2b* is the first gene identified to play a role in establishing AP asymmetry in KV, which suggests an important link between the embryonic axes.

AP asymmetry in KV

Alignment of the DV, AP and LR axes is essential for normal embryo development. The involvement of asymmetric flow in LR patterning provides a mechanism – via tight regulation of cilia position – for orienting the LR axis with the pre-existing AP and DV axes. In the mouse, it has been proposed that a posterior positioning of cilia in node cells is necessary to establish a leftward fluid flow with respect to the AP and DV axes (Buceta et al., 2005; Nonaka et al., 2005; Okada et al., 2005). However, consistent localization of cilia to the posterior pole of the KV cells has not been observed in zebrafish (Okabe et al., 2008). We propose that the relative AP position of LR ciliated cells is crucial for generating asymmetric flow in zebrafish. Analyses of the cellular architecture of KV in conjunction with quantitative measurements of fluid flow indicates that a high density of ciliated cells in the anterior region propels strong leftward flow across the anterior pole of KV, whereas fewer cilia in the posterior region return the fluid left to right (Fig. 8A). This coordinated action of asymmetrically arranged cells thereby transforms counterclockwise flow in a closed organ into a regional asymmetric flow. With regard to LR signaling, anterior leftward flow in zebrafish appears similar to flow dynamics described in mouse, rabbit and medaka (Okada et al., 2005). We suggest that strong leftward flow in the anterior region of KV is responsible for biasing *spaw* expression to left LPM (Fig. 8A) and triggering Nodal-Lefty-Pitx2 signaling. However, we cannot rule out a function for slow left-to-right flow in the posterior region of KV.

We have found that the Rho kinase Rock2b is required for AP patterning of KV. MO knockdown of *rock2b* resulted in a random distribution of LR ciliated cells (~50%) among the anterior and posterior regions of KV (Fig. 8B). This correlated with slow and uncoordinated fluid flow in KV and aberrant initiation of *spaw* expression – often bilaterally symmetric – in LPM (Fig. 8B). A reduction in the total average flow velocity in *rock2b* MO embryos (Fig. 6E) probably reflects the loss of accelerated flow in the anterior region (Fig. 6D) owing to KV architectural defects. However, we also observed abnormal beating of some (22%) LR cilia in *rock2b* MO embryos (see Movie 3 in the supplementary material). It is unclear whether these cilia beating abnormalities are separable from defects in KV architecture. The cilia beating defects may be due to the misplacement of ciliated cells in KV. Alternatively, independent targets of Rock2b may differentially control KV cell distribution and cilia beating in a subset of KV cells. To address whether flow defects correlated with the presence of abnormal cilia beating, we simultaneously imaged cilia motion and bead flow in KV. In *rock2b* MO embryos in which we observed normal cilia beating, flow was uncoordinated (see Movie 4 in the supplementary material). This suggests that even if cilia beat normally, this is not sufficient to drive coordinated flow in these embryos. Although cilia defects may contribute to the reduction of flow velocity, our results suggest that the asymmetric placement of LR cilia along the AP axis is necessary to generate coordinated flow in KV.

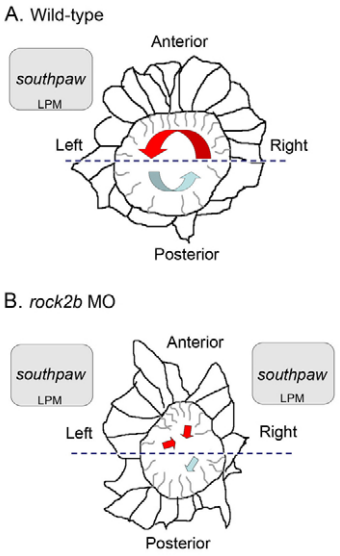

Fig. 8. Model of the relationship between KV architecture, fluid flow and asymmetric gene expression in wild-type and *rock2b* knockdown embryos. (**A**,**B**) Diagrams of KV cells traced from confocal images of T*g*(*d*usp6:*m*emGFP)^{pt19} transgenic embryos with representative cilia projecting into the KV lumen. (A) In wild-type embryos, a dense packing of elongated ciliated cells in the anterior half of KV (delineated by the dashed line) drives strong leftward flow (red arrow), and fewer cilia in the posterior half of KV move fluid rightward at a slower velocity (blue arrow). We propose anterior leftward fluid flow in KV triggers asymmetric *spaw* expression in left LPM. (B) *rock2b* MO knockdown disrupted KV cell morphology and placement along the AP axis, such that ciliated cells were equally distributed in the anterior and posterior regions. This alteration of KV architecture resulted in randomized flow direction and similar flow velocities in the anterior (red arrows) and posterior (blue arrow) regions. Disruption of KV architecture and asymmetric fluid flow resulted in abnormal initiation of *spaw* in LPM, which was frequently bilaterally symmetric.

How does Rho kinase signaling modulate KV architecture?

Live imaging of KV in *Tg*(*dusp6:memGFP*)^{pt19} embryos revealed cell morphology defects in *rock2b* morphants, such that ciliated cells failed to pack tightly into the anterior pole of KV (Fig. 8B). Rho kinase activity is known to regulate changes in the actin-myosin cytoskeleton. In mice, knockout of *Rock1* or *Rock2* results in eyelid open at birth and open abdominal wall (omphalocele) phenotypes, thought to result from failure of actin bundle assembly (Shimizu et al., 2005; Thumkeo et al., 2005). We did not find reproducible differences in the assembly or localization of actin structures in KV cells between *rock2b* MO and control embryos (Fig. 7A-F), suggesting that Rock2b regulates cytoskeletal dynamics other than assembly in KV. One of the best-characterized targets of Rho kinase is myosin light chain phosphatase (MLCP). Activated Rho kinase phosphorylates MLCP to inhibit phosphatase activity, thereby facilitating interaction between myosin and actin cytoskeleton and increasing cell contractility (Riento and Ridley, 2003). Thus, *rock2b* knockdown would be expected to result in increased MLCP activity and reduced contractility. We hypothesize Rock2b controls contractility of the actin-myosin cytoskeleton in KV cells to modulate cell shapes that are necessary for the AP arrangement of ciliated cells.

PCP signaling is a good candidate pathway for controlling Rock2b activity in KV (Kim and Han, 2005; Marlow et al., 2002; Winter et al., 2001; Zhu et al., 2006). The vertebrate PCP pathway is a non-canonical Wnt signaling cascade that can modulate the actin cytoskeleton via small GTPases including Rho (Strutt, 2001) to control polarized cell behaviors such as CE movements and orientation of stereocilia in the inner ear (Wang and Nathans, 2007). In zebrafish, MO knockdown of the Wnt receptor Frizzled2 or dominant negative interference with the Wnt signaling molecule Dishevelled (Dvl) resulted in apical actin cytoskeleton defects, and fewer and shorter cilia in KV (Oishi et al., 2006). However, *rock2b* knockdown does not alter apical actin or cilia length or number in KV, suggesting *rock2b* may function in a distinct PCP pathway. Consistent with this idea, PCP signaling has recently been shown to mediate positioning of cilia without affecting ciliogenesis. Loss of the PCP signaling proteins Inversin (Okada et al., 2005), Dvl (Hashimoto et al., 2010) or Van Gogh (Vangl) (Song et al., 2010) in mutant mice had no affect on cilia formation, but disrupted posterior positioning of LR cilia in node cells. In addition, maternal-zygotic mutant zebrafish lacking all Vangl2 function developed normal cilia, but the posterior projection of KV cilia was perturbed (Borovina et al., 2010), and MO knockdown of Vangl2 in *Xenopus* altered posterior positioning of cilia in the gastrocoel roof plate (Antic et al., 2010). Further investigation is necessary to determine whether Rho kinase-regulated morphologies of KV cells are controlled by PCP signals.

In summary, we show the zebrafish Rho kinase Rock2b is required for AP positioning of ciliated cells in KV and subsequent LR patterning in LPM and developing organs. Our results provide potential links between PCP pathways, cytoskeletal dynamics and KV cell arrangement. In addition, this study suggests a role for the ciliated KV in the alignment of the AP and LR axes during embryogenesis.

Acknowledgements

We thank F. Foley, G. Molina, H. Codore and M. Karthikeyan for technical assistance, members of the Turner lab for reagents and discussion, and C. Gao for helpful comments on the manuscript. This work was funded by an NIH NRSA postdoctoral fellowship and an AHA Scientist Development Grant to J.D.A. and by an NHLBI grant to H.J.Y. M.T.'s laboratory is supported by the NHLBI HL088016. Deposited in PMC for release after 12 months.

Competing interests statement

The authors declare no competing financial interests.

Supplementary material

Supplementary material for this article is available at
http://dev.biologists.org/lookup/suppl/doi:10.1242/dev.052985/-/DC1

References

Albertson, R. C., Yan, Y. L., Titus, T. A., Pisano, E., Vacchi, M., Yelick, P. C., Detrich, H. W., 3rd and Postlethwait, J. H. (2010). Molecular pedomorphism underlies craniofacial skeletal evolution in Antarctic notothenioid fishes. *BMC Evol. Biol.* **10**, 4.

Amack, J. D. and Yost, H. J. (2004). The T box transcription factor no tail in ciliated cells controls zebrafish left-right asymmetry. *Curr. Biol.* **14**, 685-690.

Amack, J. D., Wang, X. and Yost, H. J. (2007). Two T-box genes play independent and cooperative roles to regulate morphogenesis of ciliated Kupffer's vesicle in zebrafish. *Dev. Biol.* **310**, 196-210.

Antic, D., Stubbs, J. L., Suyama, K., Kintner, C., Scott, M. P. and Axelrod, J. D. (2010). Planar cell polarity enables posterior localization of nodal cilia and left-right axis determination during mouse and Xenopus embryogenesis. *PLoS One* **5**, e8999.

Borovina, A., Superina, S., Voskas, D. and Ciruna, B. (2010). Vangl2 directs the posterior tilting and asymmetric localization of motile primary cilia. *Nat. Cell. Biol.* **12**, 407-412.

Buceta, J., Ibanes, M., Rasskin-Gutman, D., Okada, Y., Hirokawa, N. and Izpisua-Belmonte, J. C. (2005). Nodal cilia dynamics and the specification of

the left/right axis in early vertebrate embryo development. *Biophys. J.* **89**, 2199-2209.
Chen, J. N., van Eeden, F. J., Warren, K. S., Chin, A., Nusslein-Volhard, C., Haffter, P. and Fishman, M. C. (1997). Left-right pattern of cardiac BMP4 may drive asymmetry of the heart in zebrafish. *Development* **124**, 4373-4382.
Cooper, M. S. and D'Amico, L. A. (1996). A cluster of noninvoluting endocytic cells at the margin of the zebrafish blastoderm marks the site of embryonic shield formation. *Dev. Biol.* **180**, 184-198.
Danos, M. C. and Yost, H. J. (1995). Linkage of cardiac left-right asymmetry and dorsal-anterior development in Xenopus. *Development* **121**, 1467-1474.
Danos, M. C. and Yost, H. J. (1996). Role of notochord in specification of cardiac left-right orientation in zebrafish and Xenopus. *Dev. Biol.* **177**, 96-103.
Essner, J. J., Branford, W. W., Zhang, J. and Yost, H. J. (2000). Mesendoderm and left-right brain, heart and gut development are differentially regulated by pitx2 isoforms. *Development* **127**, 1081-1093.
Essner, J. J., Amack, J. D., Nyholm, M. K., Harris, E. B. and Yost, H. J. (2005). Kupffer's vesicle is a ciliated organ of asymmetry in the zebrafish embryo that initiates left-right development of the brain, heart and gut. *Development* **132**, 1247-1260.
Hamada, H., Meno, C., Watanabe, D. and Saijoh, Y. (2002). Establishment of vertebrate left-right asymmetry. *Nat. Rev. Genet.* **3**, 103-113.
Hashimoto, H., Rebagliati, M., Ahmad, N., Muraoka, O., Kurokawa, T., Hibi, M. and Suzuki, T. (2004). The Cerberus/Dan-family protein Charon is a negative regulator of Nodal signaling during left-right patterning in zebrafish. *Development* **131**, 1741-1753.
Hashimoto, M., Shinohara, K., Wang, J., Ikeuchi, S., Yoshiba, S., Meno, C., Nonaka, S., Takada, S., Hatta, K., Wynshaw-Boris, A. et al. (2010). Planar polarization of node cells determines the rotational axis of node cilia. *Nat. Cell. Biol.* **12**, 170-176.
Ishizaki, T., Naito, M., Fujisawa, K., Maekawa, M., Watanabe, N., Saito, Y. and Narumiya, S. (1997). p160ROCK, a Rho-associated coiled-coil forming protein kinase, works downstream of Rho and induces focal adhesions. *FEBS Lett.* **404**, 118-124.
Kim, G. H. and Han, J. K. (2005). JNK and ROKalpha function in the noncanonical Wnt/RhoA signaling pathway to regulate Xenopus convergent extension movements. *Dev. Dyn.* **232**, 958-968.
Kimmel, C. B., Ballard, W. W., Kimmel, S. R., Ullmann, B. and Schilling, T. F. (1995). Stages of embryonic development of the zebrafish. *Dev. Dyn.* **203**, 253-310.
Kramer-Zucker, A. G., Olale, F., Haycraft, C. J., Yoder, B. K., Schier, A. F. and Drummond, I. A. (2005). Cilia-driven fluid flow in the zebrafish pronephros, brain and Kupffer's vesicle is required for normal organogenesis. *Development* **132**, 1907-1921.
Krauss, S., Concordet, J. P. and Ingham, P. W. (1993). A functionally conserved homolog of the Drosophila segment polarity gene hh is expressed in tissues with polarizing activity in zebrafish embryos. *Cell* **75**, 1431-1444.
Kreiling, J. A., Williams, G. and Creton, R. (2007). Analysis of Kupffer's vesicle in zebrafish embryos using a cave automated virtual environment. *Dev. Dyn.* **236**, 1963-1969.
Long, S., Ahmad, N. and Rebagliati, M. (2003). The zebrafish nodal-related gene southpaw is required for visceral and diencephalic left-right asymmetry. *Development* **130**, 2303-2316.
Marlow, F., Topczewski, J., Sepich, D. and Solnica-Krezel, L. (2002). Zebrafish Rho kinase 2 acts downstream of Wnt11 to mediate cell polarity and effective convergence and extension movements. *Curr. Biol.* **12**, 876-884.
Melby, A. E., Warga, R. M. and Kimmel, C. B. (1996). Specification of cell fates at the dorsal margin of the zebrafish gastrula. *Development* **122**, 2225-2237.
Meno, C., Shimono, A., Saijoh, Y., Yashiro, K., Mochida, K., Ohishi, S., Noji, S., Kondoh, H. and Hamada, H. (1998). lefty-1 is required for left-right determination as a regulator of lefty-2 and nodal. *Cell* **94**, 287-297.
Molina, G. A., Watkins, S. C. and Tsang, M. (2007). Generation of FGF reporter transgenic zebrafish and their utility in chemical screens. *BMC Dev. Biol.* **7**, 62.
Nasevicius, A. and Ekker, S. C. (2000). Effective targeted gene 'knockdown' in zebrafish. *Nat. Genet.* **26**, 216-220.
Noma, K., Oyama, N. and Liao, J. K. (2006). Physiological role of ROCKs in the cardiovascular system. *Am. J. Physiol. Cell Physiol.* **290**, C661-C668.
Nonaka, S., Tanaka, Y., Okada, Y., Takeda, S., Harada, A., Kanai, Y., Kido, M. and Hirokawa, N. (1998). Randomization of left-right asymmetry due to loss of nodal cilia generating leftward flow of extraembryonic fluid in mice lacking KIF3B motor protein. *Cell* **95**, 829-837.
Nonaka, S., Yoshiba, S., Watanabe, D., Ikeuchi, S., Goto, T., Marshall, W. F. and Hamada, H. (2005). De novo formation of left-right asymmetry by posterior tilt of nodal cilia. *PLoS Biol.* **3**, e268.
Odenthal, J. and Nusslein-Volhard, C. (1998). fork head domain genes in zebrafish. *Dev. Genes Evol.* **208**, 245-258.
Oishi, I., Kawakami, Y., Raya, A., Callol-Massot, C. and Izpisua Belmonte, J. C. (2006). Regulation of primary cilia formation and left-right patterning in zebrafish by a noncanonical Wnt signaling mediator, duboraya. *Nat. Genet.* **38**, 1316-1322.
Okabe, N., Xu, B. and Burdine, R. D. (2008). Fluid dynamics in zebrafish Kupffer's vesicle. *Dev. Dyn.* **237**, 3602-3612.
Okada, Y., Takeda, S., Tanaka, Y., Belmonte, J. C. and Hirokawa, N. (2005). Mechanism of nodal flow: a conserved symmetry breaking event in left-right axis determination. *Cell* **121**, 633-644.
Oteiza, P., Koppen, M., Concha, M. L. and Heisenberg, C. P. (2008). Origin and shaping of the laterality organ in zebrafish. *Development* **135**, 2807-2813.
Panizzi, J. R., Jessen, J. R., Drummond, I. A. and Solnica-Krezel, L. (2007). New functions for a vertebrate Rho guanine nucleotide exchange factor in ciliated epithelia. *Development* **134**, 921-931.
Ramsdell, A. F. (2005). Left-right asymmetry and congenital cardiac defects: getting to the heart of the matter in vertebrate left-right axis determination. *Dev. Biol.* **288**, 1-20.
Raya, A. and Belmonte, J. C. (2006). Left-right asymmetry in the vertebrate embryo: from early information to higher-level integration. *Nat. Rev. Genet.* **7**, 283-293.
Riento, K. and Ridley, A. J. (2003). Rocks: multifunctional kinases in cell behaviour. *Nat. Rev. Mol. Cell. Biol.* **4**, 446-456.
Schweickert, A., Weber, T., Beyer, T., Vick, P., Bogusch, S., Feistel, K. and Blum, M. (2007). Cilia-driven leftward flow determines laterality in Xenopus. *Curr. Biol.* **17**, 60-66.
Shimizu, Y., Thumkeo, D., Keel, J., Ishizaki, T., Oshima, H., Oshima, M., Noda, Y., Matsumura, F., Taketo, M. M. and Narumiya, S. (2005). ROCK-I regulates closure of the eyelids and ventral body wall by inducing assembly of actomyosin bundles. *J. Cell Biol.* **168**, 941-953.
Song, H., Hu, J., Chen, W., Elliott, G., Andre, P., Gao, B. and Yang, Y. (2010). Planar cell polarity breaks bilateral symmetry by controlling ciliary positioning. *Nature* **466**, 378-382.
Strutt, D. (2001). Planar polarity: getting ready to ROCK. *Curr. Biol.* **11**, R506-R509.
Thermes, V., Grabher, C., Ristoratore, F., Bourrat, F., Choulika, A., Wittbrodt, J. and Joly, J. S. (2002). I-SceI meganuclease mediates highly efficient transgenesis in fish. *Mech. Dev.* **118**, 91-98.
Thisse, B., Pflumio, S., Fürthauer, M., Loppin, B., Heyer, V., Degrave, A., Woehl, R., Lux, A., Steffan, T., Charbonnier, X. Q. and Thisse, C. (2001). Expression of the zebrafish genome during embryogenesis. *ZFIN Direct Data Submission* (http://zfin.org).
Thumkeo, D., Shimizu, Y., Sakamoto, S., Yamada, S. and Narumiya, S. (2005). ROCK-I and ROCK-II cooperatively regulate closure of eyelid and ventral body wall in mouse embryo. *Genes Cells* **10**, 825-834.
Wang, Y. and Nathans, J. (2007). Tissue/planar cell polarity in vertebrates: new insights and new questions. *Development* **134**, 647-658.
Wei, L., Roberts, W., Wang, L., Yamada, M., Zhang, S., Zhao, Z., Rivkees, S. A., Schwartz, R. J. and Imanaka-Yoshida, K. (2001). Rho kinases play an obligatory role in vertebrate embryonic organogenesis. *Development* **128**, 2953-2962.
Westerfield, M. (1995). *The Zebrafish Book*. Eugene, OR: University of Oregon Press.
Winter, C. G., Wang, B., Ballew, A., Royou, A., Karess, R., Axelrod, J. D. and Luo, L. (2001). Drosophila Rho-associated kinase (Drok) links Frizzled-mediated planar cell polarity signaling to the actin cytoskeleton. *Cell* **105**, 81-91.
Yelon, D., Horne, S. A. and Stainier, D. Y. (1999). Restricted expression of cardiac myosin genes reveals regulated aspects of heart tube assembly in zebrafish. *Dev. Biol.* **214**, 23-37.
Yost, H. J. (1999). Diverse initiation in a conserved left-right pathway? *Curr. Opin. Genet. Dev.* **9**, 422-426.
Zernicka-Goetz, M., Pines, J., Ryan, K., Siemering, K. R., Haseloff, J., Evans, M. J. and Gurdon, J. B. (1996). An indelible lineage marker for Xenopus using a mutated green fluorescent protein. *Development* **122**, 3719-3724.
Zhang, Y., Li, X., Qi, J., Wang, J., Liu, X., Zhang, H., Lin, S. C. and Meng, A. (2009). Rock2 controls TGFbeta signaling and inhibits mesoderm induction in zebrafish embryos. *J. Cell Sci.* **122**, 2197-2207.
Zhu, S., Liu, L., Korzh, V., Gong, Z. and Low, B. C. (2006). RhoA acts downstream of Wnt5 and Wnt11 to regulate convergence and extension movements by involving effectors Rho kinase and Diaphanous: use of zebrafish as an in vivo model for GTPase signaling. *Cell Signal* **18**, 359-372.